Diabatic crossing of chiral "twins" in the odd-odd ^{106}Ag nucleus: A theoretical perspective

Sham S. Malik*
Department of Physics, Guru Nanak Dev University, Amritsar-143005, India
(Received 10 December 2015; revised manuscript received 3 May 2016; published 29 July 2016)

A systematic study of both the observed positive-parity magnetic rotation band and the negative-parity $\Delta I = 1$ doublet bands in an odd-odd ^{106}Ag nucleus is carried out. The negative-parity doublet bands depict some unusual features that have not been observed in any isotope in the mass $A = 100$ region. For instance, (i) the moment of inertia of the partner band is quite different from that of the yrast band, and (ii) these bands cross each other at an angular momentum of $I = 14\hbar$. Also, the observed significantly large but constant $B(M1)$ transitions confirm that the strong $M1$ transitions are being reinforced by the contributions from collective rotation. To explain these features, a collective model has been developed whose kinetic and potential energies are extracted from the tilted-axis cranking model. Instead of the triaxial parameter γ, a second-order phase transition is found to be responsible for the spontaneous breakdown of chiral symmetry. Analytical solution of the Schrödinger equation has generated a doublet nondegenerate eigenvalue spectrum. The ensuing model results based on the two-quasiparticle configuration $\pi g_{\frac{9}{2}} \otimes \nu h_{\frac{11}{2}}$ exhibit similarities with many observed features of the negative-parity doublet bands and hence confirm their chiral character. The cranking mass parameter in kinetic energy plays an important role in diabatic crossing between these emerged chiral twin bands.

DOI: 10.1103/PhysRevC.94.014324

I. INTRODUCTION

The occurrence of chirality in nuclear physics was first suggested in 1997 by Frauendorf and Meng [1] and is expected to occur in nuclei having triaxial shapes. Petrache *et al.* [2] have reported a pair of $\Delta I = 1$ bands with same parity in ^{134}Pr, which have been interpreted by Frauendorf and Meng [1] as a first candidate for chiral twin bands. These bands arise mainly due to the possible existence of two enantiomeric (left- and right-handed) forms of the nucleus. Since then a large number of experimental investigations have been undertaken to establish the existence of chiral twin bands in several mass regions of nuclear landscape [3–8]. It is emphasized that the observed doublet must have identical or, in practice, very similar rotational spectra, spin alignments, and electromagnetic transition probabilities.

In the year 2007, Joshi and co-workers [9] have observed some novel features of the negative-parity $\Delta I = 1$ doublet bands in the ^{106}Ag nucleus. For example, the moment of inertia of the partner band is quite different from that of the yrast band and these bands cross each other at an angular momentum, $I \sim 14\hbar$. Such a unique characteristic, i.e., diabatic crossing of the doublet at a particular angular momentum, has not yet been observed in other nuclei in the mass $A \sim 100$ region [3,10–14]. In favor of different moments of inertia, they have suggested that the main and partner bands originate, respectively, from the triaxial and the axially symmetric shapes. Therefore, the shape transformation induced by chiral vibration has been given as a possible explanation for a planar axial rotation band being a partner of a triaxial band. Although the chiral "twins" have energies close to each other, it is rare to observe a crossing between them. An additional characteristic of chiral bands is that their in-band $B(M1)$ and $B(E2)$ values as well as their $B(M1)/B(E2)$ ratios should be identical [15,16]. Recently, the Tata Institute of Fundamental Research group [17] has observed identical $B(M1)$ and $B(E2)$ transition probabilities in both these bands and has fully supported the claim of Joshi *et al.* [9].

The triaxial deformation, which is a key ingredient of chiral rotation, was investigated for the negative-parity $\Delta I = 1$ doublet bands in ^{106}Ag by Ma and co-workers [18]. They have revealed that the main and the partner bands in this nucleus do not correspond to two different shapes (i.e., triaxial and axially symmetric), but rather these bands correspond to magnetic rotation (MR) bands based on two different quasiparticle configurations, namely: $\pi(g_{\frac{9}{2}})^1 \otimes \nu(h_{\frac{11}{2}})^1$ (for the main band) and $\pi(g_{\frac{9}{2}})^1 \otimes \nu(h_{\frac{11}{2}})^3$ (for the partner band). Alternatively, Lieder and co-workers [19] in their more recent investigation have drawn similar conclusions but with a different four-quasiparticle configuration $[\pi(g_{\frac{9}{2}})^1 \otimes \nu((g_{\frac{7}{2}}/d_{\frac{5}{2}})^2 h_{\frac{11}{2}})]$ for the partner band. Both these works have rejected the proposal of Joshi *et al.* [9]. The absence of triaxiality in ^{106}Ag brings up questions regarding its chiral rotation.

Thus, the above analyses have emphasized two contrasting possibilities for the negative-parity $\Delta I = 1$ doublet bands in the ^{106}Ag isotope, i.e., (i) the chiral twins emerging from shape transformation and (ii) the MR bands based on two distinct quasiparticle configurations. However, direct evidence for the existence of a generalized triaxial shape in a nuclear system is not possible, because two different deformation parameters β (quadrupole deformation) and γ (an extent of departure from the symmetric shape) cannot be extracted from a single experimental $B(E2, I \rightarrow I - 2)$ value. Further, similar $B(E2)$ values for the observed doublet do not support the two different quasiparticles picture. Therefore, the explanation corresponding to chiral twins cannot be completely ruled out. To resolve this paradox and to get an insight into the origin of different moments of inertia of these doublet bands, I have developed a model parallel to the collective model of Chen *et al.* [20].

*shammalik@yahoo.com

Before proceeding to strengthen my viewpoint, I would like to mention an important aspect related to chiral symmetry. Recently, Bhattacharya and Kleinert [21] have discussed the chiral symmetries in both two- and three-dimensional angular momentum systems. Their simple model calculations clearly reveal that the chiral structures prevail not only in a three-dimensional angular momentum system Hamiltonian but also in a two-dimensional angular momentum system Hamiltonian.

Dimitrov and co-workers [22] have established the chiral character in an odd-odd ^{134}Pr nucleus on the basis of the nonplanar tilted-axis cranking (TAC) calculations. Their self-consistent minimization of the Routhian has fixed the bandhead of chiral partner bands in a planar configuration. This means at low spin, the proton-particle prefers to combine with the neutron-hole in a plane and leads to two-degenerate TAC solutions with the tilt angles θ and $(\pi - \theta)$. Correspondingly, a $\Delta I = 1$ band is supported at the bandhead. Higher spins in their TAC solutions emerge from the nonplanar angular momentum distributions. In this way, two planar TAC solutions bifurcate onto four nonplanar ones with an increase in rotational frequency. Thus, the nonplanar TAC solutions have generated a pair of identical $\Delta I = 1$ bands of same parity. Because triaxial nuclei are generally γ soft, it is not yet clear whether the TAC solutions corresponding to a planar configuration at higher spins fulfill the self-consistent constraint. On the other hand, it is quite possible that a planar TAC solution fulfills that self-consistent constraint accurately. The present calculations of positive-parity bands (Sec. II B) have reflected the testing limit of self-consistent minimization. Further, because the TAC approach is based on the mean-field theory, the description of quantum tunneling between the identical doublet $\Delta I = 1$ bands is not possible [23,24].

To describe the energy splitting between the chiral twin bands, one has to go beyond the mean-field approximation. Numerous efforts in this direction have already been carried out by various authors [25–27]. Alternatively, Chen and co-workers [20] have developed the collective model for explaining the prominent features of chiral twin bands. They have established the collective Hamiltonian by extracting the potential energy and mass parameter from the TAC model. In their approach, they have realized for the first time the importance of the double-well potential (DWP) for the emergence of chiral structures.

The DWP of a physical system is generally expressed as $V_{\rm DWP} = -\alpha\phi^2 + \lambda\phi^4$, where α and λ are positive constants and ϕ is a variable of a quantum mechanical state. This potential has two sets of extrema, i.e., $\phi_0 = 0$ and $\phi_0 = \pm\sqrt{\frac{\alpha}{2\lambda}}$. The minima are located at $\phi_0 = \pm\sqrt{\frac{\alpha}{2\lambda}} = \langle 0|\phi|0\rangle$, rather than at $\phi_0 = 0$. This means that the energy at $\phi_0 = \pm\sqrt{\frac{\alpha}{2\lambda}}$ is lower than that at $\phi_0 = 0$. Therefore, $\phi_0 = 0$ corresponds to the normal state while $\langle 0|\phi|0\rangle = \pm\sqrt{\frac{\alpha}{2\lambda}}$ are the stable ground states of the physical system. Also, these two ground states satisfy $\langle 0|\phi|0\rangle \neq -\langle 0|\phi|0\rangle$ under the transformation $\phi \to -\phi$. That is, the symmetry of the ground states has been destroyed. Obviously, this spontaneous breakdown of symmetry occurs due to the nonlinear term $\lambda\phi^4$ in the potential. According to Landau's theory of phase transition, the system undergoes a second-order phase transition in such a case where the normal state $\phi_0 = 0$ changes to the stable ground state $\langle 0|\phi|0\rangle = \pm\sqrt{\frac{\alpha}{2\lambda}}$. Recently, it has been established that a single $\Delta I = 1$ band that is developed in the left well at time $t = 0$ tunnels to the right well of opposite handedness with the evolution of time [28]. Further, the tunneling through the DWP lifts the degeneracy between the rotational partners.

The main aim of the present paper is to establish the chiral character of the negative-parity $\Delta I = 1$ doublet bands in the ^{106}Ag nucleus. The collective Hamiltonian for a system of one $g_{\frac{9}{2}}$ proton-hole and one $h_{\frac{11}{2}}$ neutron-particle coupled to a triaxial rigid rotor is constructed. The potential energy and mass parameters involved in the collective Hamiltonian are extracted from the TAC model. Instead of the triaxial parameter γ, a second-order phase transition is found to be responsible for the spontaneous breakdown of chiral symmetry. Analytical solution of the Schrödinger equation has generated a doublet nondegenerate eigenvalue spectra. The ensuing model results exhibit similarities with many observed features of the negative-parity doublet bands and hence ensure their chiral character. The cranking mass parameter in kinetic energy is found to play an important role in diabatic crossing between these emerged chiral twin bands.

A complete model of the TAC developed by Frauendorf may be found in Ref. [29]. In Sec. II A, a brief account of the TAC model is presented for completeness. Because the mass $A \sim 110$ region is quite prone to both MR bands [30–34] and chiral twin bands [3,10,12]. Therefore, the ^{106}Ag nucleus may also be considered to lie in the island of magnetic-dipole and chiral twin bands. He and co-workers [35] have already claimed the magnetic rotation character in the positive-parity $\Delta I = 1$ band. In Sec. II B, I have also analyzed this positive parity MR band using the TAC model. Section II C highlights the contributions of TAC in the observed negative-parity doublet bands in ^{106}Ag. The collective model is developed in Sec. II D. The results and discussions are presented in Sec. III. Finally, the conclusions are summarized in Sec. IV.

II. THEORETICAL FORMALISM

Many calculations have been reported in the literature both for the MR and the chiral doublet bands on the basis of a multiparticle version of the TAC model where pairing and residual interactions have also been included [22,24,29,36]. In an odd-odd ^{106}Ag isotope, both the MR (positive-parity) band and the suspected negative-parity chiral twins are observed [9,35] side by side. First, I investigate both these phenomena by using the TAC model and pinpoint the similarities and dissimilarities between theory and observed data. A very brief outline of this model is presented, which is barely necessary to support the following discussion. This model has already been used by me and my colleagues to explain the observed features of the MR bands [37–39].

A. Tilted-axis cranking model

Within the pairing plus quadrupole-quadrupole interaction, the quasiparticle Routhian [29] is given by

$$h' = h_{\rm sp} - \hbar\omega_0\beta\left[\cos\gamma q_0 - \frac{\sin\gamma}{\sqrt{2}}(q_2 + q_{-2})\right] - \Delta(P^+ + P) - \lambda n - \vec{\omega}\cdot\vec{j}, \quad (1)$$

with $\vec{\omega} \cdot \vec{j} = \omega(j_1 \sin\theta \cos\phi + j_2 \sin\theta \sin\phi + j_3 \cos\theta)$. Here, $h_{\rm sp}$ is the single-particle Hamiltonian of a deformed field (e.g., a deformed oscillator or a deformed Woods-Saxon potential); ω is the cranking frequency; θ and ϕ are the tilt angles of the resultant angular momentum with respect to the principal 3-axis and 1-axis, respectively; and j_i ($i = 1$ to 3) are the components of the particle angular momentum $\vec{j}$ along the three axes, where the 3-axis is the symmetry axis. Further, $\hbar\omega_0 = \frac{41}{A^{\frac{1}{3}}}$ MeV, β and γ are the usual deformation parameters. q_0, q_2, and q_{-2} are the expectation values of the respective components of the quadrupole tensor Q. The operator P^+ creates the pair field, the strength of which is fixed by the gap parameter Δ. In the following calculations, the proton and neutron pairing gap parameters have been chosen as 80% of the experimental odd-even mass difference and are calculated by using the expressions given in Ref. [40] with the binding energies taken from the atomic mass tables [41]. The Fermi level is fixed to give an average particle number at the cranking frequency $\omega = 0$.

The total Routhian $E'(\omega)$ is calculated by using the Strutinsky renormalization technique [42]:

$$E'(\omega) = E_{\rm LD} - E_{\rm smooth} + \langle\omega|h'|\omega\rangle. \qquad (2)$$

Here, $E_{\rm LD}$ is the liquid-drop energy and the smooth part of the energy, $E_{\rm smooth}$, is calculated by the Strutinsky averaging method. The deformation parameters (ϵ_2, ϵ_4, and γ) and the tilt angles (θ and ϕ) are found self-consistently by minimizing the total Routhian $E'(\omega)$ for a given frequency and a chosen configuration.

B. Analysis of positive-parity MR band

The Beijing group [35] has studied the high-spin states in the ^{106}Ag nucleus and has identified the MR character in the positive-parity $\Delta I = 1$ band on the basis of the TAC model. Parallel to this study, I have also carried out the TAC calculations for this band just to test the self-consistent constraint. A self-consistent solution (corresponding to each variable in the Hamiltonian) is the one at which the total angular momentum $\langle\vec{j}\rangle$ is parallel to the angular frequency $\vec{\omega}$ [43]. Once the self-consistent constraint is fulfilled, the Routhian attains a minimum value for a given set of parameters.

In the observed positive-parity MR band in ^{106}Ag [35], the bandhead spin I^Π is 13^+, which indicates the multi-quasiparticle character of the band. Taking the bandhead spin and parity into consideration, I have chosen a four-quasiparticle configuration,

$$\{\pi(g_{\frac{9}{2}}) \otimes \nu[(h_{\frac{11}{2}})^2(g_{\frac{7}{2}}/d_{\frac{5}{2}})]\},$$

similar to that of Ref. [35]. Using the constant values of Δ_p (=0.893 MeV), Δ_n (=0.739 MeV), and ω (=0.15 MeV), a self-consistent minimization determines the deformation parameters ϵ_2, ϵ_4, and γ, respectively, as 0.144, 0.0, and 5.1°. Because $\gamma \ll 30°$, a nearly prolate shape with an average tilt angle of $\theta \sim 70°$ emerges.

Figure 1 shows the plot of the angular momentum I vs the rotational frequency $\hbar\omega$ of the calculated data (solid line) along with the experimental data (solid circles connected by a solid line). The calculated bandhead is nearly one unit higher than that of the observed one. The overall trend of the experimental data is reproduced nicely. The following points clearly support the MR character in this band.

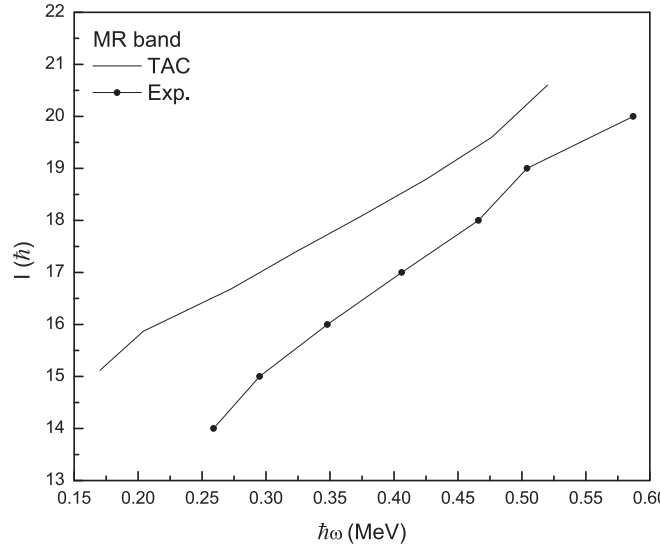

FIG. 1. The calculated angular momentum I vs the rotational frequency $\hbar\omega$ for the positive-parity MR band in ^{106}Ag. Solid circles connected with a solid line represent the experimental data.

(i) The observed bandhead (I^Π is 13^+) excitation energy is greater than 2 MeV.
(ii) The calculated deformation parameter ($\epsilon_2 \sim 0.14$) is extremely small.
(iii) A major part of the total angular momentum originates from the coupling of the angular momenta of valence protons and neutrons through the shear mechanism.
(iv) Similar configuration, i.e.,

$$\{\pi(g_{\frac{9}{2}}) \times \nu[(h_{\frac{11}{2}})^2(g_{\frac{7}{2}}/d_{\frac{5}{2}})]\},$$

based bands have already been identified as magnetic rotation bands in the neighboring ^{104}Ag [44] and ^{108}Ag [45] isotopes.

I would like to mention here that the angular momentum I vs the rotational frequency $\hbar\omega$ plot (Fig. 1) shows behavior similar to that of Fig. 4 in Ref. [35]. This similarity supports the testing limit of the self-consistent minimization procedure adopted in the present calculations. Also, an interesting point is that the trend of a small but rather constant moment of inertia of the MR band is fully supported by both these calculations.

Further, the reduced transition probabilities are calculated by using the following semiclassical expressions:

$$B(M1, \Delta I = 1) = \frac{3}{8\pi}(\mu_3 \sin\theta - \mu_1 \cos\theta)^2 \qquad (3)$$

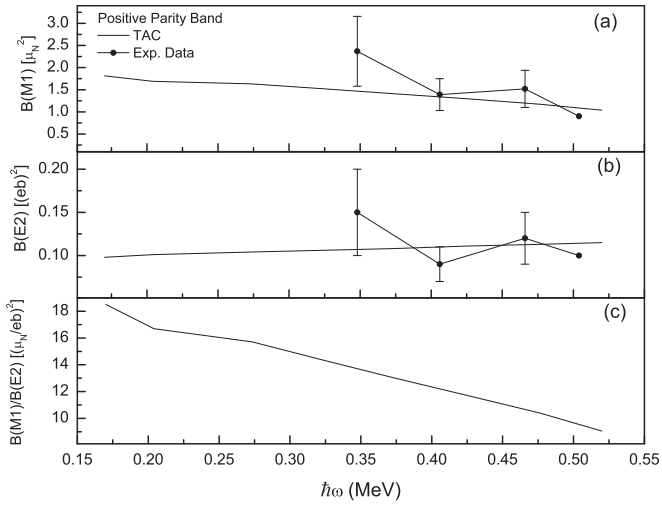

FIG. 2. (a) The calculated $B(M1)$ values. (b) The calculated $B(E2)$ values. (c) The calculated ratio $B(M1)/B(E2)$ vs the rotational frequency $\hbar\omega$ for the positive-parity configuration. Experimental data with error bars from Ref. [47] are also plotted as solid circles.

and

$$B(E2,\Delta I=2)=\frac{15}{128\pi}\left(Q_0{}'\sin^2\theta+\sqrt{\frac{2}{3}}Q_2{}'\left(1+\cos^2\theta\right)\right)^2. \quad (4)$$

Here, μ's are the expectation values of the corresponding operator of the magnetic dipole moment and Q''s are the expectation values of the intrinsic quadrupole moment operator. The expectation values of the proton and neutron spins are attenuated by a factor of 0.7 for the calculations of $B(M1)$ values. The microscopic reason for this attenuation factor is not fully understood. A general observation reveals that the calculated $B(M1)$ values reproduce the experimental data with the standard attenuation factor of 0.6–0.7 for the spin part of the magnetic transition moments. In a relativistic framework, this corresponds to an attenuation of the anomalous gyromagnetic ratio [46].

These transition probabilities vs the rotational frequency $\hbar\omega$ are shown in Fig. 2 and are compared with the available experimental data [47]. The calculated $B(M1)$ values and the experimental data are shown in Fig. 2(a). Both the observed and the calculated $B(M1)$ values lie between 1 and 2 $\mu_N{}^2$ and show a decreasing trend with an increasing rotational frequency and hence with an increasing angular momentum I. This decreasing behavior with an increasing rotational frequency ensures the validity of the shear mechanism in this positive-parity band. Further, the calculated $B(E2)$ values together with the observed data are shown in Fig. 2(b). Both the observed and calculated values are of the order of $\sim$0.1 $(eb)^2$. These extremely small constant values of $B(E2)$ also ensure its MR character. Finally, the $B(M1)/B(E2)$ ratios are plotted in Fig. 2(c). It may be seen that the calculated ratio $B(M1)/B(E2)$ lies between 19 and 9 $(\mu_N/eb)^2$, thus indicating the in-band transitions are predominantly $M1$ in character. Also, this ratio decreases with an increasing angular momentum, which is again an indication of the shear mechanism in this band.

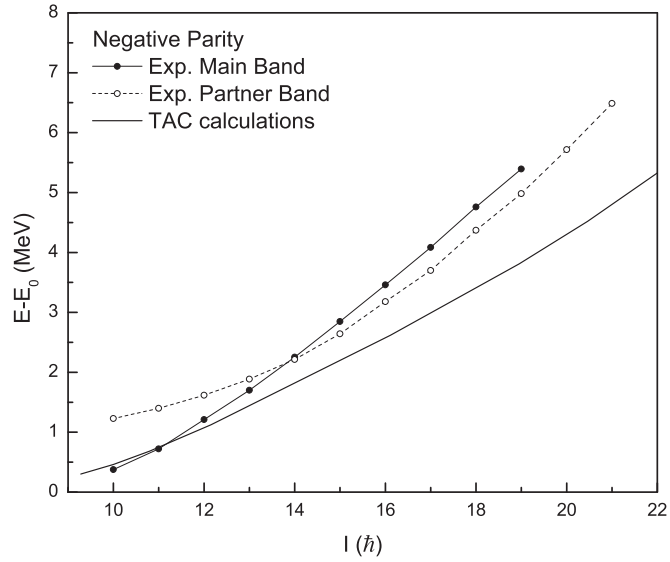

FIG. 3. The normalized experimental excitation energy E-E_0 (MeV) vs the angular momentum I for the negative-parity doublet bands. The normalization E_0 refers to the excitation energy of the $I^\Pi = 9^-\hbar$ level of the main band. Here, solid and open circles represent, respectively, the observed main and partner bands. The calculated excitation spectra normalized to $I^\Pi = 8.55^-\hbar$ are shown as a solid line.

C. Analysis of negative-parity doublet bands

The observed structures of the negative-parity main (solid circles connected with a solid line) and partner (open circles connected with a dashed line) bands are shown in Fig. 3. Here, the excitation energies plotted on the ordinate are normalized with respect to the energy E_0 of the $I^\Pi = 9^-\hbar$ level of the main band. This plot reveals that (i) the moments of inertia of the two bands are quite different and (ii) these bands cross each other at an angular momentum of $I = 14\hbar$.

Before going to analyze these negative-parity doublet bands, I would like to point out that the mass $A \sim 110$ region falls in a γ-soft domain. Such transitional nuclei may have shallow minima at finite γ deformation in the Hartree-Fock-Bogoliubov calculations [48]. It has been demonstrated that such shallow minima become prominent ones when projected onto spin $I = 0\hbar$ [49]. Thus, to describe these transitional nuclei, it is important to consider the basis states $|\epsilon_2,\epsilon_4,\gamma,\theta,\phi\rangle$ (which are the eigenstates of the triaxial mean-field potential) rather than the axial basis. Shi and co-workers [50] have already tested the validity of self-consistent constraint in γ-soft nuclei by considering sufficient basis states in their TAC model space.

For the analysis of the observed negative-parity doublet $\Delta I = 1$ bands, three major harmonic shells ($N = 3$–6) for each type of nucleon have been used. These shells are quite sufficient in constructing an appropriate model space for the mass $A \sim 110$ region. I carry out the TAC calculations for

these bands by choosing a two-quasiparticle configuration, $\pi(g_{\frac{9}{2}}) \otimes \nu(h_{\frac{11}{2}})$, as suggested by Joshi *et al.* [9]. The self-consistent minimization of the Routhian (2) fixes the deformation parameters as $\epsilon_2 = 0.172$, $\epsilon_4 = 0.04$, and $\gamma = 4.8^\circ$. In these calculations, the constant values of Δ_p (=0.893 MeV) and Δ_n (=0.739 MeV) are considered throughout the band. The nucleus (^{106}Ag) discussed here contains an odd number of protons and neutrons. It is well known that the pairing effects for such nuclei get reduced by the blocked high-j orbitals near the Fermi surface. Also, this pairing keeps on decreasing gradually with an increase in rotational frequency. Therefore, the variation of the pairing strength parameter (Δ_n and/or Δ_p) is quite essential at each rotational frequency. In the present formalism, I have not carried out the self-consistent minimization of the Routhian (2) at higher rotational frequency and, also, the variation of the pairing strength parameters has not been carried out for the following reasons.

(i) These calculations consume a lot of computer time.
(ii) Dimitrov and co-workers [22] have made the TAC calculations for the odd-odd ^{134}Pr nucleus with constant pairing strength parameters. Further, they have noticed that the planar states contribute to the bandhead spin of chiral twin bands. The present calculation also supports a planar configuration and reproduces the bandhead spin of negative-parity $\Delta I = 1$ bands.
(iii) Oi and Walker [51] have already noticed that self-consistent minimization does not support a stable aplanar configuration.
(iv) In the subsequent discussion, I have considered these negative-parity doublets as quasirotational with considerable vibrational contribution.

Thus, a single $\Delta I = 1$ negative parity band is supported on a planar configuration. The calculated excitation energy E (MeV) is normalized with respect to the energy E_0 of state $I = 8.55\hbar$ and is plotted in Fig. 3 as a solid line. A comparison with the experimental plots reveals the following interesting points.

(i) The observed bandhead of the main band is reproduced nicely with an assigned two-quasiparticle configuration, $[\pi(g_{\frac{9}{2}}) \otimes \nu(h_{\frac{11}{2}})]$. Because the triaxial parameter γ in the TAC calculation comes out to be 4.8°, which is much less than the triaxial value 30°, it completely rules out the possibility of triaxial shape for this main band as claimed by Joshi *et al.* [9].
(ii) The calculated excitation spectrum, which was initially close to the observed main band, subsequently becomes closer to the partner band at an angular momentum of $I = 14\hbar$.

An important aspect of this plot is that the calculated spectrum follows either the main band or the partner band, whichever is lowest in excitation energy over a considerable range of angular momentum. Thus, the minimum excitation spectrum extracted out of two observed rotational bands follows closely the calculated spectrum based on the two-quasiparticle configuration $\pi(g_{\frac{9}{2}}) \otimes \nu(h_{\frac{11}{2}})$. Therefore, the possibility of two different quasiparticle configurations for these bands is not an appropriate option. This remarkable observation clearly rules out the possibility that these observed bands have a MR characterbased on two different quasiparticle configurations that were already claimed by two different groups [18,19]. In the subsequent discussion, the absence of MR character in these bands is also supported by the observed $B(M1)$ transition probability.

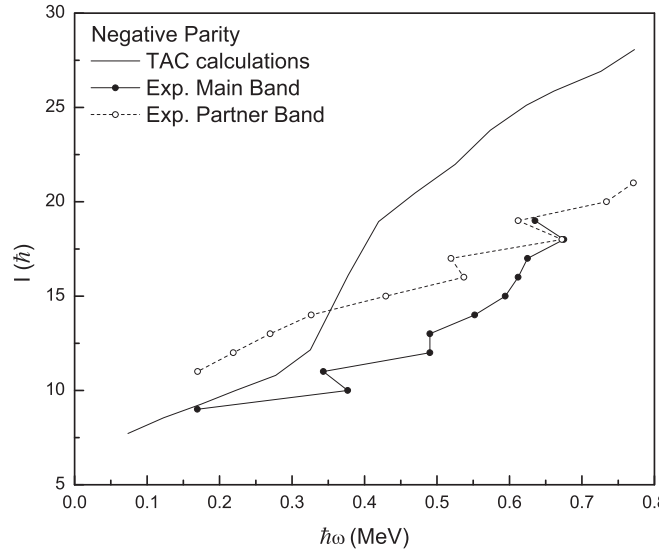

FIG. 4. The calculated angular momentum I vs the rotational frequency $\hbar\omega$ for the negative-parity configuration (solid line). Experimental data for the main band (solid circles connected with a solid line) and the partner band (open circles connected with a dashed line) are also shown.

To confirm the above claim further, I plot in Fig. 4 the calculated as well as the experimental data of the angular momentum I vs the rotational frequency $\hbar\omega$. On comparing the observed γ-ray energies with those of TAC calculations, it is clear that the lower portion of the main band is better reproduced in terms of magnitude and trend. Also, the trend of a higher portion of the observed partner band is reproduced reasonably well above the angular momentum $I \sim 14\hbar$ by same two-quasiparticle configuration based band.

Further, the experimental and calculated $B(M1)$ values are compared in the upper panel of Fig. 5. It is noticed in this plot that the calculated $B(M1)$ values agree reasonably well with the observed $B(M1)$ values of the main and partner bands over a considerable range of angular momentum. A remarkable point to be noticed here is that the calculated as well as the observed $B(M1)$ values stay nearly constant over the considered range of angular momentum; i.e., these values do not decrease with increasing angular momentum as expected for the MR phenomenon. This completely rules out the possibility of the shear mechanism prevailing in both the main and partner bands. Also, the significantly large but constant magnitudes of the observed $B(M1)$ values ensure that the strong $M1$ transitions are being reinforced by the contributions from the collective rotation. Hence, the possibility of collective rotation is still alive.

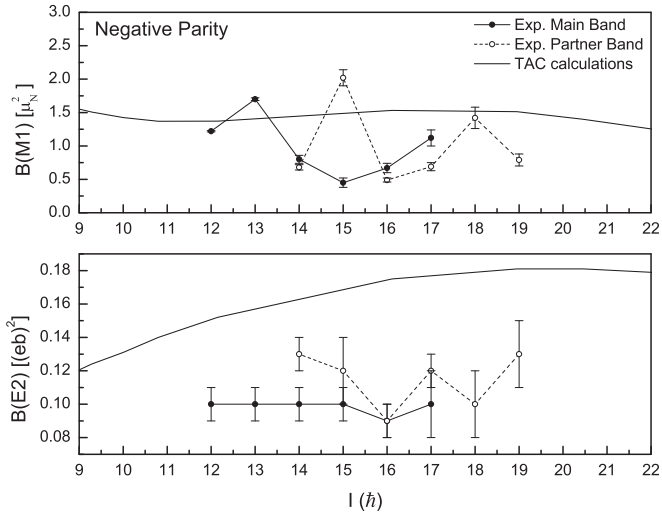

FIG. 5. Upper panel: A solid line shows the calculated $B(M1)$ values vs the angular momentum I for the negative-parity configuration. Experimental data for the main band (solid circles) and the partner band (open circles) are also shown. Lower panel: $B(E2)$ values with the same description.

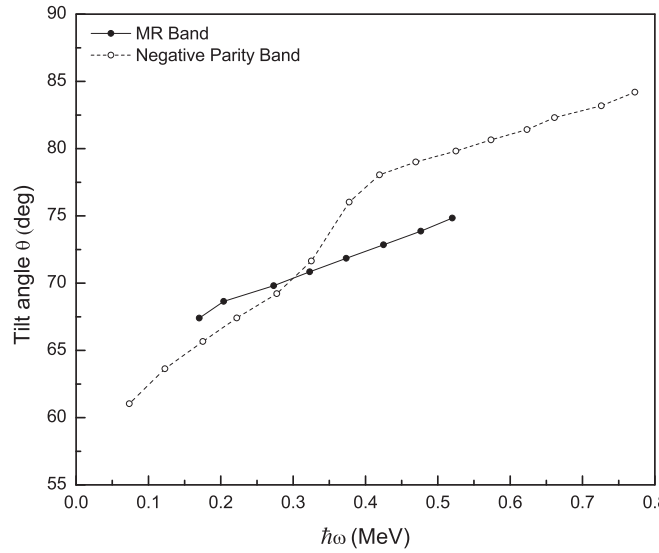

FIG. 6. Variation of the tilt angle θ vs the rotational frequency $\hbar\omega$ both for positive- and negative-parity configurations.

In the lower panel Fig. 5, the experimental and calculated $B(E2)$ values are plotted. Within the error bars, nearly the same observed values of the main and partner bands completely rule out the possibilities of two different configurations for these bands. These observed $B(E2)$ values are nearly constant and are quite small over the observed range of angular momentum. Therefore, these values favor small deformation for these bands as obtained in the TAC calculation ($\epsilon_2 = 0.172$). The TAC model results also show a nearly constant behavior over the considered range of angular momentum and are consistent with the observed trend. However, the calculated $B(E2)$ values are significantly larger than those of the observed ones. It is worthwhile to pinpoint that, in these calculations, a self-consistent minimization of the Routhian is carried out near the bandhead rotational frequency. The self-consistent minimization at higher rotational frequency may increase the triaxiality parameter γ (because ^{106}Ag nucleus is γ soft in character). Schnare and co-workers [52] did the TAC calculations for γ-soft nuclei in the mass $A \sim 80$ region and noticed that $B(E2)$ values decrease by a factor of 2 with an increase of γ from $0^\circ \leqslant \gamma \leqslant 20^\circ$. Hence, the self-consistent minimization at higher rotational frequencies may improve the agreement between the theoretical and experimental $B(E2)$ values. This observation clearly supports the triaxiality at higher rotational frequencies.

Thus, both the possibilities, i.e., shape transition (from triaxial to axially symmetric) and the MR character based on two different quasiparticle configurations (from two to four) for the observed main and partner bands, are not supported by the TAC model calculations. It is worthwhile to mention here that the experimental $B(M1)$ values for both these bands are nearly constant over a considerable range of angular momentum. This constant behavior supports the collective rotation rather than the shear mechanism for the observed $M1$ transitions. This point is also supported by Fig. 6 in which the tilt-angle θ is plotted vs the rotational frequency $\hbar\omega$ for both the positive-parity MR band and the negative-parity configuration band. It is quite evident from this plot that the MR band as usual depends weakly on the tilt angle whereas the tilt angle varies strongly with the rotational frequency for the negative-parity band. Similar conclusions for the MR and high-K bands have already been drawn by Frauendorf [29]. Still the paradoxical situation prevails, so I have developed a collective model parallel to Chen and co-workers [20] for the analysis of negative-parity doublet bands.

D. Collective model for negative-parity doublet

The collective model Hamiltonian for the two-quasiparticle negative-parity configuration $\pi(g_{\frac{9}{2}}) \otimes \nu(h_{\frac{11}{2}})$ is constructed on the basis of the TAC model by extracting the potential energy and the mass parameter as follows. Following Chen and co-workers [20], the potential energy is obtained by minimizing the total Routhian (2) with respect to $\theta(\omega)$ and is given by

$$V(\theta) = E'(\theta) - \frac{1}{2}\sum_k \Im_k {\omega_k}^2, \tag{5}$$

where k varies between 1 and 3 and $\Im_k = \Im_0 \sin^2(\gamma - \frac{2\pi}{3}k)$ with $\Im_0 = 40\hbar^2/\text{MeV}$ being the moment of inertia along the k axis. Because the potential $V(\theta)$ has minima at finite nonvanishing values of θ, in this case, the nucleus ^{106}Ag can exhibit rotations that can be described by the time-dependent parameter $\theta(t)$ in the laboratory frame. Therefore, these rotations have been considered as collective ones.

Following the guidelines of Chen and co-workers [20], the quantized form of collective Hamiltonian, using the Pauli prescription [53], can be expressed as

$$H_{\text{coll}} = -\frac{\hbar^2}{2\sqrt{B(\theta)}}\frac{\partial}{\partial\theta}\Big[\frac{1}{\sqrt{B(\theta)}}\frac{\partial}{\partial\theta}\Big] + V(\theta). \tag{6}$$

The mass parameter $B(\theta)$ for the kinetic energy term is consistently calculated by using the TAC model states in the adiabatic cranking formula based on the BCS formalism (see Refs. [54,55] for details). For the present calculations, the following form of the cranking mass formula has been chosen:

$$B(\theta) = 2\hbar^2 \sum_{\mu,\nu>0} \frac{\langle\mu|\frac{\partial H}{\partial\theta}|\nu\rangle\langle\nu|\frac{\partial H}{\partial\theta}|\mu\rangle}{(\tilde{\epsilon_\mu} + \tilde{\epsilon_\nu})^3}(u_\mu v_\nu + u_\nu v_\mu)^2. \tag{7}$$

In Eq. (7), $|\mu\rangle$ denotes the single-particle states of the TAC model. I would like to mention here that a range of three harmonic oscillator shells ($N = 3$–6) for an individual nucleon is quite sufficient for calculating the self-consistent deformation parameters ϵ_2, ϵ_4, and γ and it also saves computer time. On the other hand, the mass parameter calculations require more than three oscillator shells for an individual nucleon, so $N = 0$ to 9 harmonic oscillator shells have been chosen for these calculations. Such a large configuration space usually does not change the equilibrium deformation parameters obtained within three oscillator shells. The inclusion of a large configuration space, particularly at low deformation, ensures that cutoff levels lie very far from the Fermi level and hence overcome the divergences. Here, u_μ and v_μ correspond to the BCS occupation numbers and $\tilde{\epsilon_\mu}$ represents the quasiparticle energy.

Thus, knowing the potential and mass parameters, the stationary Schrödinger equation in variable θ can be expressed as

$$\left[-\frac{\hbar^2}{2\sqrt{B(\theta)}}\frac{\partial}{\partial\theta}\left(\frac{1}{\sqrt{B(\theta)}}\frac{\partial}{\partial\theta}\right) + V(\theta)\right]\Psi^\nu(\theta) = E^\nu\Psi^\nu(\theta). \tag{8}$$

Chen and co-workers [20] have solved the Schrödinger equation (8) by using box boundary conditions and have obtained the analytical expressions for both positive- and negative-parity eigenstates. Instead of an analytical solution, Eq. (8) is solved numerically and the probability $|\Psi^\nu(\theta)|^2$ of angular distribution is thus obtained. The normalized angular distribution is given by

$$P[\theta(I)] = |\Psi^\nu(\theta)|^2\sqrt{B(\theta)}, \tag{9}$$

with the constraint

$$\int_{\theta_{\min}}^{\theta_{\max}} P(\theta)d\theta = 1. \tag{10}$$

The states $\Psi^\nu(\theta)$ are the vibrational states in the potential $V(\theta)$, counted by the quantum number $\nu = 0, 1, 2, ...$ Here, each quantum number ν supports a rotational band. If only the yrast state is permissible and there is complete adiabaticity, then only $\nu = 0$ contributes in Eq. (8). These states may arise mainly due to interaction between $\theta(\omega)$ and other deformation degrees of freedom. Higher vibrational states are nearly equally spaced (i.e., vibrational character) and are counted by higher values of $\nu = 1, 2, 3, ...$However, if the system (^{106}Ag) is nonyrast, then higher values of ν will contribute.

III. RESULTS AND DISCUSSION

A self-consistent minimization of the total Routhian $E'[\theta(\omega)]$ is used in obtaining the potential energy $V(\theta)$ [Eq. (5)] and is shown in the upper panel of Fig. 7. This potential varies smoothly as a function of the tilt angle θ. Using the single-particle states corresponding to each $\theta(\omega)$ value, the cranking masses $B(\theta)$ are obtained by using expression (7) and are shown in the lower panel of Fig. 7. The observed structure in the mass parameter arises mainly due to the presence of shell effects in single-particle states. Using these potential and cranking masses, the normalized angular distributions [Eq. (9)] for the first two excited states and the ground state are shown in Fig. 8. Here, the ground state corresponds to the vibrational degree of freedom $\nu = 0$ with energy $E^0 \sim 3$ MeV and the first and second excited states refer to $\nu = 1$ (with $E^1 \sim 7$ MeV) and 2 (with $E^2 \sim 12$ MeV), respectively. I would like to mention here that these excited states do not correspond to different configurations, but arise mainly due to the presence of vibrational states in potential. The following discussion [given in point (iii)] clearly highlights the emergence of these vibrational states and each vibrational state supports an individual rotational spectrum.

It is remarkable to notice here that a unique crossing between the ground state (solid circles connected with a solid line) and the first excited state (open circles connected with a dashed line) occurs at an angular momentum of $I = 15\hbar$. On the other hand, the second excited state (triangles connected with a dotted line) crosses the ground state at multiple points without any similarity in their angular momentum. The following important points emerge from this plot.

(i) The second excited state angular distribution does not compete (in magnitude) with that of the first excited state or even the ground-state distribution except for a few angular momenta. This observation completely rules out the possibility of the existence of a second excited negative-parity $\Delta I = 1$ band based on the

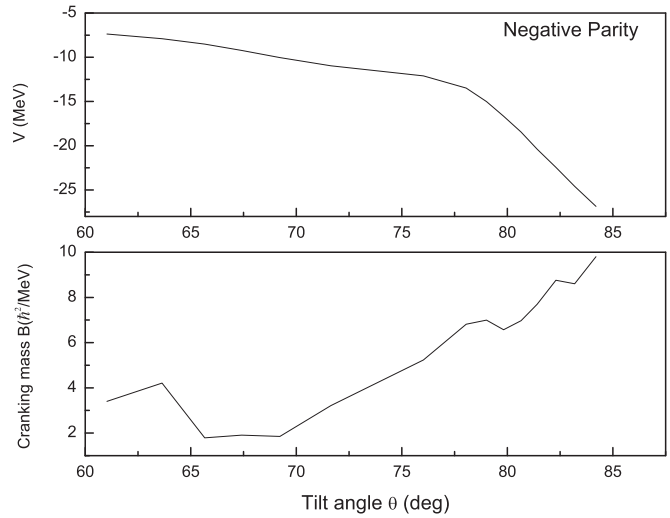

FIG. 7. Upper panel: The potential energy $V(\theta)$ in MeV vs the tilt angle θ. Lower panel: The variation of cranking masses.

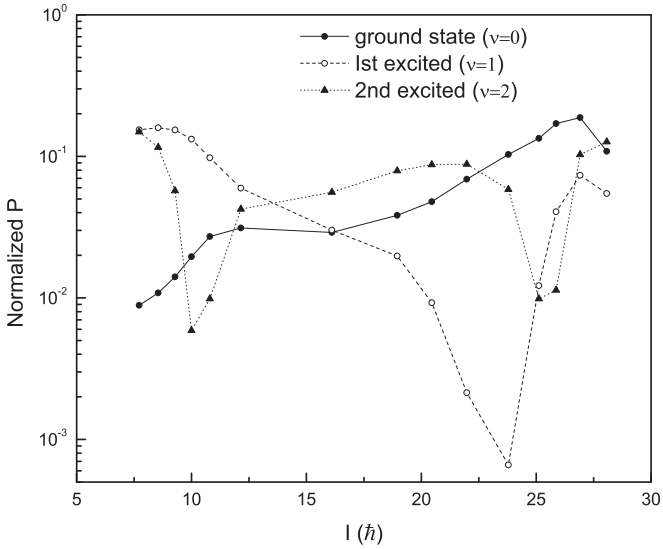

FIG. 8. The normalized angular distribution for the ground state (solid circles connected with a solid line), the first excited state (open circles connected with a dashed line), and the second excited state (triangles connected with a dotted line) vs the angular momentum I for the negative-parity configuration. Here, the energy of the ground state $\nu = 0$ is ∼3 MeV and that of the first ($\nu = 1$) and second excited states ($\nu = 2$) are, respectively, ∼7 and ∼12 MeV.

same two-quasiparticle configuration $\pi(g_{\frac{9}{2}}) \otimes \nu(h_{\frac{11}{2}})$ in the ^{106}Ag nucleus. More recently, Lieder and co-workers [19] have observed negative-parity Band 3 (see Fig. 1 in Ref. [19]) and have claimed the four-quasiparticle configuration $\pi(g_{\frac{9}{2}}) \otimes \nu[(d_{\frac{5}{2}}/g_{\frac{7}{2}})^2 h_{\frac{11}{2}}]$ for this band. Thus, both theory and experimental outcome are consistent with each other.

(ii) The probability of the first excited state distribution is higher than that of the ground state till $I \leqslant 15\hbar$. Just after this angular momentum reverse trend (i.e., excited state distribution becomes lower than that of the ground state) follows a considerable range of angular momentum. This implies that within the angular momentum range $I_b \leqslant I < 15\hbar$, the first excited state spectrum is more probable as compared to that of the yrast state. The higher probability of the first excited state spectrum ensures that the ground states are being fed by the excited states within the angular momentum range $I_b \leqslant I < 15\hbar$. This result is fully consistent with the observed feeding pattern prevailing between two negative-parity bands [9].

(iii) It is worthwhile to mention here that the crossing between the ground state ($\nu = 0$) and first excited-state ($\nu = 1$) angular distributions at an angular momentum of $I = 15\hbar$ has a direct relevance with that of the observed rotational spectra of the main and partner bands. This point is more vivid from the following simple analysis. It has already been pointed out that in a planar configuration, two degenerate TAC solutions at θ and $(\pi - \theta)$ have generated a negative-parity $\Delta I = 1$ band. Its potential, $V(\theta)$, and mass parameter, $B(\theta)$, are shown, respectively, in the upper and lower panels of Fig. 7. Both of these (potential and mass parameter) can be well approximated as harmonic in character, like

$$V(\theta) = \tfrac{1}{2}k\theta^2, \quad B(\theta) = \tfrac{1}{2}p\theta^2, \tag{11}$$

with k and p as constants. Substituting these expressions for $V(\theta)$ and $B(\theta)$ in Eq. (8), one finds that

$$\frac{d^2\Psi}{d\theta^2} - \frac{1}{\theta}\frac{d\Psi}{d\theta} - (a\theta^4 - b\theta^2)\Psi = 0, \tag{12}$$

with $a = \frac{pk}{2\hbar^2}$ and $b = \frac{pE}{\hbar}$. Equation (12) has two linearly independent solutions for a given energy E:

$$\Psi_1(\theta) = \sqrt{b - a\theta^2}\, J_{\frac{1}{3}}\left(\frac{\left(\sqrt{b - a\theta^2}\right)^3}{a}\right), \tag{13}$$

$$\Psi_2(\theta) = \sqrt{b - a\theta^2}\, J_{-\frac{1}{3}}\left(\frac{\left(\sqrt{b - a\theta^2}\right)^3}{a}\right). \tag{14}$$

Here, $J_q(\theta)$ is a Bessel function of order q. Each zero of the Bessel function supports a rotational spectrum, because the rotational spectrum varies with $\theta(\omega)$. Here, the first node supports a yrast spectrum, whereas the excited spectra are supported by higher nodes. It is noticed that the yrast and first excited rotational spectra follow a parabolic character and a constant separation prevails between two spectra. The main reason for this constant separation is that the fluctuations in the mass parameters due to shell effects have been ignored. Hence, the shell effects in mass parameters play a dominant role in diabatic crossing between the main and partner bands.

Because the present formalism is based on the guidelines of the collective model of Chen and co-workers [20], it is worthwhile to highlight the significant achievements in comparison to those of the collective model [20]. These points are more vivid from the following analytical treatment of the Schrödinger equation (8).

A. Comparison with the collective model of Chen and co-workers [20]

Chen and co-workers [20] have realized for the first time the importance of the double-well-potential (DWP) for obtaining the energy splitting between the chiral doublet bands. In their formalism, they have fixed the triaxiality parameter ($\gamma = -30^\circ$) and have obtained the potential energy and mass parameter of Eq. (8) for each rotational frequency. A symmetric DWP is seen at each rotational frequency. I have obtained a similar DWP by using an alternative procedure that is discussed below.

By defining the modified wave function

$$\Phi = \frac{1}{\sqrt{B(\theta)}}\Psi^{\nu}, \tag{15}$$

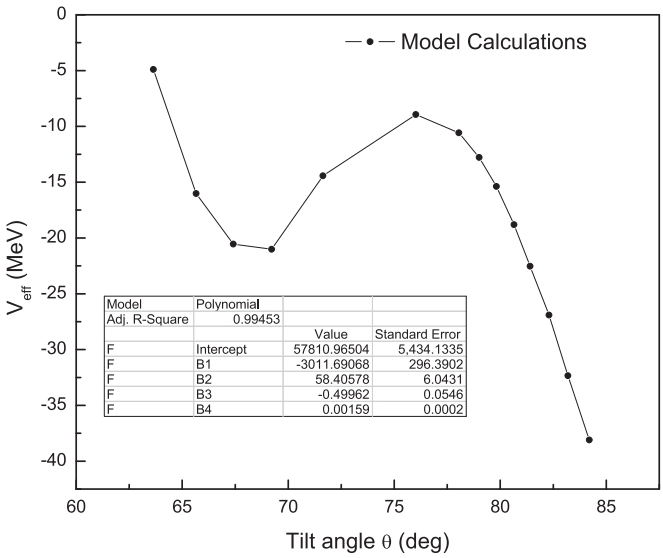

FIG. 9. The effective potential energy $V_{\rm eff}(\theta)$ in MeV vs the tilt angle θ is plotted. The quartic polynomial fit to the calculated potential is made. The fitting parameters are listed also and the error in each polynomial fit parameter is less than 10%.

corresponding to the eigenvalue $\Lambda = E^{\nu}$, Eq. (8) reduces to the simplest form

$$-\frac{\hbar^2}{2B(\theta)}\frac{\partial^2\Phi(\theta)}{\partial\theta^2}+\left[V(\theta)+\frac{\hbar^2}{2B^{\frac{3}{4}}(\theta)}\frac{\partial^2}{\partial\theta^2}\sqrt{\frac{1}{\sqrt{B(\theta)}}}\right]\Phi(\theta) = \Lambda\Phi(\theta). \tag{16}$$

All the terms in the square brackets are a function of the collective variable θ and together make up the effective potential

$$V_{\rm eff}(\theta) = V(\theta)+\frac{\hbar^2}{2B^{\frac{3}{4}}(\theta)}\frac{\partial^2}{\partial\theta^2}\sqrt{\frac{1}{\sqrt{B(\theta)}}}. \tag{17}$$

The effective potential $V_{\rm eff}(\theta)$ is plotted in Fig. 9 (solid circles connected with a dotted line). It is quite interesting to notice that the quartic polynomial fits this potential nicely. The fitting parameters are listed in this figure and an error in each parameter is less than 10%. By an appropriate transformation, this quartic polynomial can also be expressed as

$$V_{\rm eff}(\theta) = V_0-\alpha(\theta-\theta_0)^2+\lambda(\theta-\theta_0)^4, \tag{18}$$

with the constants $\alpha > 0$ and $\lambda > 0$. The appearance of a negative sign in the quadratic term ensures the double-well character of the potential $V_{\rm eff}(\theta)$ [Eq. (18)] with the central maximum at $\theta = \theta_0$. I would like to mention here that an asymmetry in the DWP arises mainly due to the following two reasons.

(i) The calculation of cranking masses is quite sensitive to the pairing contribution. In the TAC model calculations, a constant pairing strength parameter for both protons and neutrons (i.e., Δ_p and Δ_n) is used. Apparently, this pairing strength should vary with the variation in cranking frequency. A self-consistent minimization of the Routhian (2) with varying Δ_p and Δ_n may partially remove the asymmetry in DWP.

(ii) A constant value of the moment of inertia $\Im_0$ ($= 40\hbar^2$/MeV) is used in obtaining the potential energy (5). It is well known that the moment of inertia should vary with the angular momentum [56]. Therefore, an appropriate choice of a variable moment of inertia in lieu of $\Im_0$ is required for removing the asymmetry in DWP.

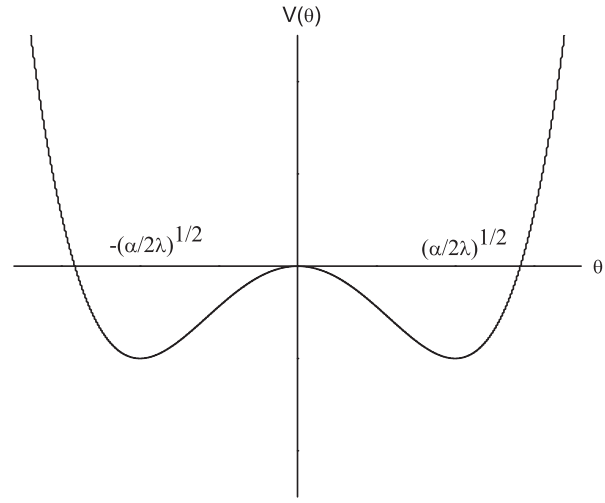

FIG. 10. The symmetric double-well potential for the potential vs the tilt angle θ.

Inclusion of both these factors may help in generating the symmetric DWP around the central maximum θ_0. Symmetry of the DWP is required just to fulfill the constraint of parity conservation.

Considering an appropriate renormalization and shifting the central maximum θ_0 to origin, a symmetric DWP is shown in Fig. 10. Symmetry of the DWP ensures the parity conservation. Under these simplifications, Eq. (16) becomes

$$\frac{d^2\Phi}{d\theta^2}+\frac{2B(\theta)}{\hbar^2}[\Lambda - V_{\rm eff}(\theta)]\Phi(\theta) = 0, \tag{19}$$

with $V_{\rm eff}(\theta) = -\alpha\theta^2+\lambda\theta^4$.

This effective potential has two sets of extrema, $\theta = 0$ and $\theta_{\pm} = \pm\sqrt{\frac{\alpha}{2\lambda}}$, and stable minima are located at $\theta_{\pm} = \pm\sqrt{\frac{\alpha}{2\lambda}}$ rather than at $\theta = 0$. These two ground states do not obey $U(1)$ symmetry. In other words, the symmetry of the ground states has been destroyed. The reason for this spontaneous breakdown of symmetry arises mainly due to the presence of the nonlinear interaction $\lambda\theta^4$ in Hamiltonian (19) of the system. According to Landau's theory of phase transition [57], the system corresponding to Hamiltonian (19) undergoes a second-order phase transition in which a normal ground state $\theta = 0$ is changed to two unusual stable ground states $\theta_{\pm} = \pm\sqrt{\frac{\alpha}{2\lambda}}$. It has already been established that the second-order phase transition is responsible for the spontaneous breakdown of chiral symmetry [28].

I would like to mention here that by fixing the triaxiality parameter ($\gamma = -30^\circ$), Chen and co-workers [20] have generated two identical ΔI bands in their aplanar configuration. These rotational bands reside in the left and right wells separately. In the present formalism, spontaneous breakdown of symmetry has developed the DWP. The planar configuration has supported a negative $\Delta I = 1$ band initially in the left well. Subsequently it tunnels to the right well with an evolution of time.

The well depth corresponding to these minima comes out to be $V_{\rm eff}(\theta_\pm) = -\frac{\alpha^2}{4\lambda}$. It is quite interesting to notice here that the positions of minima $\theta_\pm$ remain invariant whereas the well depths $V_{\rm eff}(\theta_\pm)$ vary directly with the variation of the cranking mass parameter $B(\theta)$. It has already been established that the system with symmetric DWP oscillates between two wells with frequency $\omega = \frac{\Delta E}{\hbar}$, with $\Delta E = \langle \Phi_L|\hat{H}|\Phi_R\rangle = \langle \Phi_L|\hat{H}|\Phi_R\rangle$ [28]. Here, L and R represent the left and right sides of the well, respectively. As soon as the well depth vanishes for a particular cranking mass, the system attains the superbarrier state. The tunneling through the superbarrier does not split the level and hence ΔE comes out to be zero. This result is fully consistent with the plot shown in Fig. 5 of Ref. [20], which reveals that as the barrier height increases the splitting between the rotational spectra decreases. Further, the well depth is mainly controlled by the potential and the mass parameter. Please note that both pairing and shell effects in the potential and the cranking mass parameter play a significant role in diabatic crossing between two rotational spectra in a system. This point more clearly shows up in the following expression of the eigenvalue Λ.

First, I consider $2B(\theta)/\hbar^2 = 1$ MeV^{-1} for the sake of simplicity and define

$$\Lambda - V_{\rm eff}(\theta) = x_\pm\sqrt{2\alpha} + \frac{\Xi}{8\alpha}. \tag{20}$$

To obtain the eigenvalues, one has to fix $x_\pm$ and Ξ. Within these substitutions, Eq. (19) becomes

$$\frac{d^2\Phi}{d\theta^2} + \left[x_\pm\sqrt{2\alpha} + \frac{\Xi}{8\alpha} - 2\alpha U(\theta)\right]\Phi(\theta) = 0, \tag{21}$$

where

$$U(\theta) = \frac{1}{2\alpha}(V_{\rm eff}(\theta) - V_{\rm eff}(\theta_\pm)). \tag{22}$$

One of the solutions of the second-order differential equation [Eq. (21)] near the origin to the right of the well is given by

$$\Phi_A(\theta) = \frac{|\theta-\theta_+|^{\frac{1}{2}(x_+-1)}}{|\theta+\theta_+|^{\frac{1}{2}(x_++1)}}\exp\left[-\frac{1}{\sqrt{2}}\left(\frac{\sqrt{2\lambda}}{3}\theta^3 - \frac{\alpha}{\sqrt{2\lambda}}\right)\right]. \tag{23}$$

The second solution of Eq. (21) near the origin to the left side of the well is obtained by replacing $\theta \to -\theta$, i.e., $\Phi_A(-\theta)$. For $x_+ = x_- = x_0$, both these solutions are associated with same expansion for Ξ, which is given by

$$\Xi = -2\lambda\left(3{x_0}^2+1\right) - \frac{\sqrt{2}\lambda^2}{8\alpha^{\frac{3}{2}}}x_0\left(17{x_0}^2+19\right), \tag{24}$$

with allowed values of $x_0 = (2n+1)$, $n = 0, 1, 2, ...$Hence the eigenvalue $\Lambda(0)$ is obtained by using Eq. (20). Because the solutions $\Phi_A(\theta)$ and $\Phi_A(-\theta)$ are valid around the origin $\theta = 0$, i.e., in the domain away from the minima $\theta_\pm$, their linear superpositions generate even or odd solutions about $\theta = 0$, which are given by

$$\Phi_\pm(\theta) = \tfrac{1}{2}[\Phi_A(\theta) \pm \Phi_A(-\theta)]. \tag{25}$$

Because the DWP differs from that of the simple harmonic oscillator potential in having two minima instead of one and also because it is more probable to find a particle in a region of minimum than elsewhere, it is naturally expected that the wave function there be similar to that of the harmonic oscillator. These solutions are the standard parabolic cylinder functions. These wave functions are matched with the wave functions (25) extending to minima $\theta_\pm$, i.e., $\Phi_\pm(\theta_\pm) = \frac{1}{2}[\Phi_A(\theta) \pm \Phi_A(-\theta)]_{\theta\to\theta_\pm}$, just to fix arbitrary constants. Also, the wave functions near the minima of the DWP satisfy the following two sets of boundary conditions:

$$\frac{\partial\Phi_+}{\partial\theta} = 0, \quad \Phi_+(\theta_\pm) \neq 0, \quad \Phi_-(\theta_\pm) = 0, \quad \frac{\partial\Phi_-}{\partial\theta} \neq 0, \tag{26}$$

and

$$\frac{\partial\Phi_+}{\partial\theta} \neq 0, \quad \Phi_+(\theta_\pm) = 0, \quad \Phi_-(\theta_\pm) \neq 0, \quad \frac{\partial\Phi_-}{\partial\theta} = 0. \tag{27}$$

It is worth mentioning here that Chen and co-workers [20] have used box boundary conditions for solving the Schrödinger equation (8). They have opted for these conditions because the mass parameters are significantly large at the boundary. On the other hand, the boundary conditions (26) and (27), which particularly fulfill the characteristics of the DWP, have been used. One of the reasons for this choice is that the DWP arises mainly due to the combined effect of the potential and the mass parameter. For example, the most basic solutions would be even with maxima at $\theta\pm$. However, an even wave function can also pass through zero at these points. The odd wave function then follows the exactly opposite behavior at the same time as compared to that of the even wave function.

The evaluation of these boundary conditions leads to

$$x - x_0 = \mp 4\sqrt{\frac{1}{2\pi}}\frac{2^{x_0}\left(\frac{\alpha^{\frac{3}{2}}}{\lambda}\right)^{\frac{x_0}{2}}}{2^{\frac{x_0}{4}}\left[\frac{1}{2}(x_0-1)\right]!}\exp\left[-\sqrt{\frac{2}{3}}\frac{\alpha^{\frac{3}{2}}}{\lambda}\right], \tag{28}$$

with $x_+ = x_- = x$. Further, an expansion of the eigenvalue around the integer x_0 gives

$$\Lambda = \Lambda(0) + (x-x_0)\left(\frac{\partial\Lambda}{\partial x}\right)|_{x=x_0} = \Lambda(0) + (x-x_0)\sqrt{2\alpha}. \tag{29}$$

Using Eq. (28) in this expression, two different eigenvalues, namely, $\Lambda_\pm$, are obtained. The splitting between these

eigenvalues is obtained as $\Delta\Lambda = \Lambda_- - \Lambda_+$ and is given by

$$\Delta\Lambda = 2^{\frac{(2n+13)}{4}} \frac{\sqrt{\alpha}}{\sqrt{\pi} n!} \left(\frac{4\alpha^{\frac{3}{2}}}{\lambda}\right)^{(n+\frac{1}{2})} \exp\left[-\sqrt{\frac{2}{3}}\frac{\alpha^{\frac{3}{2}}}{\lambda}\right]. \quad (30)$$

In Eq. (30), the quantum number n (=0, 1, 2, 3, ...) plays the role of the angular momentum I. Because in this derivation, $2B(\theta)/\hbar^2 = 1$ MeV^{-1} has been used, the separation between the eigenvalues $\Lambda_\pm$, i.e., $\Delta\Lambda$, varies only with the angular momentum I. For large angular momentum, this separation vanishes because the factorial form of angular momentum appears in the denominator of Eq. (30). A more realistic picture of splitting emerges if one incorporates the effect of cranking masses in Eq. (30). It is quite evident from Eq. (19) that both α and λ vary linearly with the cranking mass parameter $B(\theta)$. The appearance of an exponential term in Eq. (30) ensures that the splitting $\Delta\Lambda$ tends to zero for a large value of exponent, which mainly arises from the combined effect of the potential and the mass parameter. Both these ingredients depend on pairing and shell effects. The observed spectra, shown in Fig. 3, also support zero splitting at an angular momentum of $I = 14\hbar$.

Our earlier experience in calculating the cranking masses [58] reveals that, for the pure independent-particle motion, the values of the mass parameter obtained with Eq. (7) should be abnormally small. Indeed, these mass parameters are directly related to the derivatives of the wave functions with respect to the tilt angle. In the pure independent particle motion, these are known to be small. (An exceptional case occurs when two single-particle levels cross.) Their behavior is different when one considers residual interactions like pair correlation. With the pair correlations, the composition of the nuclear wave functions changes more strongly with the tilt angle. In this case, the increased values of mass parameters emerge in comparison with the very low values of independent particle motion. This is because as soon as some pairing correlations are present, the dependence of mass parameters on the strength of residual interaction (i.e., Δ_p and Δ_n) is much more moderate. In some cases in the deformed region, there is a significant shell in the single-particle spectrum so that the pairing gap is very small. It is then essentially the case of independent particle motion.

Thus, the calculation of cranking masses is quite sensitive to the pairing contribution. In the TAC model calculations, constant pairing strength parameters for both protons and neutrons (i.e., Δ_p and Δ_n) have been used. Apparently, this pairing strength should vary with the variation in cranking frequency. A self-consistent minimization of the Routhian (2) with varying Δ_p and Δ_n may reproduce the observed splitting behavior in the negative-parity doublet bands. Thus, the questions of (i) vanishing of splitting between the eigenvalues $\Lambda_\pm$ and (ii) reappearance of splitting in a reverse order after a critical angular momentum of $I \sim 14\hbar$ point out not only the problem of self-consistent minimization of the Routhian with Δ_p and Δ_n but also that an analytical expression for the variation of cranking masses with angular momentum is required. This apparently calls for further refinement of the present model.

IV. CONCLUSIONS

To conclude, I have carried out a complete analysis of both the positive-parity MR band and the negative-parity doublet bands observed in the ^{106}Ag nucleus. The TAC model is found to be quite successful in explaining the MR phenomenon prevailing in this nucleus. On the other hand, the unusual features of negative-parity doublet bands, for instance, (i) their different moment of inertia and (ii) a diabatic crossing between them, are explained by developing the collective model. The kinetic and potential energies of the collective Hamiltonian are extracted by using the TAC model. Instead of the triaxial parameter γ, a second-order phase transition is responsible for the spontaneous breakdown of chiral symmetry. Analytical solution of the Schrödinger equation has generated a doublet nondegenerate eigenvalue spectra. The ensuing model results based on the two-quasiparticle configuration $\pi g_{\frac{9}{2}} \otimes \nu h_{\frac{11}{2}}$ exhibit similarities with many observed features of the negative-parity doublet bands and hence confirm their chiral character. The cranking mass parameter in kinetic energy plays an important role in diabatic crossing between these emerged chiral twin bands.

[1] S. Frauendorf and J. Meng, Nucl. Phys. A **617**, 131 (1997).
[2] C. M. Petrache *et al.*, Nucl. Phys. A **597**, 106 (1996).
[3] C. Vaman, D. B. Fossan, T. Koike, K. Starosta, I. Y. Lee, and A. O. Macchiavelli, Phys. Rev. Lett. **92**, 032501 (2004).
[4] K. Starosta, T. Koike, C. J. Chiara, D. B. Fossan, D. R. LaFosse, A. A. Hecht, C. W. Beausang, M. A. Caprio, J. R. Cooper, R. Krücken, J. R. Novak, N. V. Zamfir, K. E. Zyromski, D. J. Hartley, D. Balabanski, J.-Y. Zhang, S. Frauendorf, and V. I. Dimitrov, Phys. Rev. Lett. **86**, 971 (2001).
[5] T. Koike, K. Starosta, C. J. Chiara, D. B. Fossan, and D. R. LaFosse, Phys. Rev. C **67**, 044319 (2003).
[6] A. A. Hecht, C. W. Beausang, K. E. Zyromski, D. L. Balabanski, C. J. Barton, M. A. Caprio, R. F. Casten, J. R. Cooper, D. J. Hartley, R. Krücken, D. Meyer, H. Newman, J. R. Novak, E. S. Paul, N. Pietralla, A. Wolf, N. V. Zamfir, J.-Y. Zhang, and F. Donau, Phys. Rev. C **63**, 051302 (2001).
[7] S. Zhu, U. Garg, B. K. Nayak, S. S. Ghugre, N. S. Pattabiraman, D. B. Fossan, T. Koike, K. Starosta, C. Vaman, R. V. F. Janssens, R. S. Chakrawarthy, M. Whitehead, A. O. Macchiavelli, and S. Frauendorf, Phys. Rev. Lett. **91**, 132501 (2003).
[8] S. Y. Wang *et al.*, Phys. Lett. B **703**, 40 (2011).
[9] P. Joshi, M. P. Carpenter, D. B. Fossan, T. Koike, E. S. Paul, G. Rainovski, K. Starosta, C. Vaman, and R. Wadsworth, Phys. Rev. Lett. **98**, 102501 (2007).
[10] J. Timar, C. Vaman, K. Starosta, D. B. Fossan, T. Koike, D. Sohler, I. Y. Lee, and A. O. Macchiavelli, Phys. Rev. C **73**, 011301(R) (2006).
[11] J. Timar *et al.*, Phys. Lett. B **598**, 178 (2004).
[12] P. Joshi *et al.*, Phys. Lett. B **595**, 135 (2004).
[13] J. Timár, T. Koike, N. Pietralla, G. Rainovski, D. Sohler, T. Ahn, G. Berek, A. Costin, K. Dusling, T. C. Li, E. S. Paul, K. Starosta, and C. Vaman, Phys. Rev. C **76**, 024307 (2007).

[14] P. Joshi *et al.*, Eur. Phys. J. A **24**, 23 (2005).
[15] T. Koike, K. Starosta, and I. Hamamoto, Phys. Rev. Lett. **93**, 172502 (2004).
[16] S. Y. Wang, S. Q. Zhang, B. Qi, and J. Meng, Chin. Phys. Lett. **24**, 536 (2007).
[17] N. Rather, P. Datta, S. Chattopadhyay, S. Rajbanshi, A. Goswami, G. H. Bhat, J. A. Sheikh, S. Roy, R. Palit, S. Pal, S. Saha, J. Sethi, S. Biswas, P. Singh, and H. C. Jain, Phys. Rev. Lett. **112**, 202503 (2014).
[18] H.-L. Ma, S.-H. Yao, B.-G. Dong, X.-G. Wu, H.-Q. Zhang, and X.-Z. Zhang, Phys. Rev. C **88**, 034322 (2013).
[19] E. O. Lieder *et al.*, Phys. Rev. Lett. **112**, 202502 (2014).
[20] Q. B. Chen, S. Q. Zhang, P. W. Zhao, R. V. Jolos, and J. Meng, Phys. Rev. C **87**, 024314 (2013).
[21] M. Bhattacharya and M. Kleinert, Eur. J. Phys. **35**, 025007 (2014).
[22] V. I. Dimitrov, S. Frauendorf, and F. Donau, Phys. Rev. Lett. **84**, 5732 (2000).
[23] J. Meng, J. Peng, S. Q. Zhang, and S.-G. Zhou, Phys. Rev. C **73**, 037303 (2006).
[24] S. Frauendorf, Rev. Mod. Phys. **73**, 463 (2001).
[25] S. Mukhopadhyay, D. Almehed, U. Garg, S. Frauendorf, T. Li, P. V. Madhusudhana Rao, X. Wang, S. S. Ghughre, M. P. Carpenter, S. Gros, A. Hecht, R. V. F. Janssens, F. G. Kondev, T. Lauritsen, D. Seweryniak, and S. Zhu, Phys. Rev. Lett. **99**, 172501 (2007).
[26] D. Almehed, F. Donau, and S. Frauendorf, Phys. Rev. C **83**, 054308 (2011).
[27] J. Meng and S. Q. Zhang, J. Phys. G: Nucl. Part. Phys. **37**, 064025 (2010).
[28] S. S. Malik, Nucl. Phys. A **940**, 279 (2015).
[29] S. Frauendorf, Nucl. Phys. A **557**, 259 (1993).
[30] N. S. Kelsall *et al.*, Phys. Rev. C **61**, 011301(R) (1999).
[31] C. J. Chiara, S. J. Asztalos, B. Busse, R. M. Clark, M. Cromaz, M. A. Deleplanque, R. M. Diamond, P. Fallon, D. B. Fossan, D. G. Jenkins, S. Juutinen, N. S. Kelsall, R. Krücken, G. J. Lane, I. Y. Lee, A. O. Macchiavelli, R. W. MacLeod, G. Schmid, J. M. Sears, J. F. Smith, F. S. Stephens, K. Vetter, R. Wadsworth, and S. Frauendorf, Phys. Rev. C **61**, 034318 (2000).
[32] C. J. Chiara, D. B. Fossan, V. P. Janzen, T. Koike, D. R. LaFosse, G. J. Lane, S. M. Mullins, E. S. Paul, D. C. Radford, H. Schnare, J. M. Sears, J. F. Smith, K. Starosta, P. Vaska, R. Wadsworth, D. Ward, and S. Frauendorf, Phys. Rev. C **64**, 054314 (2001).
[33] D. G. Jenkins *et al.*, Phys. Lett. B **428**, 23 (1998).
[34] D. G. Jenkins, R. Wadsworth, J. A. Cameron, R. M. Clark, D. B. Fossan, I. M. Hibbert, V. P. Janzen, R. Krucken, G. J. Lane, I. Y. Lee, A. O. Macchiavelli, C. M. Parry, J. M. Sears, J. F. Smith, and S. Frauendorf, Phys. Rev. Lett. **83**, 500 (1999).
[35] C. Y. He, L. H. Zhu, X. G. Wu, S. X. Wen, G. S. Li, Y. Liu, Z. M. Wang, X. Q. Li, X. Z. Cui, H. B. Sun, R. G. Ma, and C. X. Yang, Phys. Rev. C **81**, 057301 (2010).
[36] V. I. Dimitrov, F. Donau, and S. Frauendorf, Phys. Rev. C **62**, 024315 (2000).
[37] S. Lakshmi, H. C. Jain, P. K. Joshi Amita, P. Agarwal, A. K. Jain, and S. S. Malik, Phys. Rev. C **66**, 041303(R) (2002).
[38] S. Lakshmi, H. C. Jain, P. K. Joshi, A. K. Jain, and S. S. Malik, Phys. Rev. C **69**, 014319 (2004).
[39] S. S. Malik, P. Agarwal, and A. K. Jain, Nucl. Phys. A **732**, 13 (2004).
[40] R. Bengtsson, S. Frauendorf, and F. R. May, At. Data Nucl. Data Tables **35**, 15 (1986).
[41] A. H. Wapstra and G. Audi, Nucl. Phys. A **595**, 409 (1995).
[42] V. M. Strutinsky, Nucl. Phys. A **95**, 420 (1967).
[43] A. K. Kerman and N. Onishi, Nucl. Phys. A **361**, 179 (1981).
[44] P. Datta, S. Chattopadhyay, P. Banerjee, S. Bhattacharya, B. Dasmahapatra, T. K. Ghosh, A. Goswami, S. Pal, M. S. Sarkar, S. Sen, H. C. Jain, P. K. Joshi, and Amita, Phys. Rev. C **69**, 044317 (2004).
[45] F. R. Espinoza-Quinones *et al.*, Phys. Rev. C **52**, 104 (1995).
[46] J. A. McNeil, R. D. Amado, C. J. Horowitz, M. Oka, J. R. Shepard, and D. A. Sparrow, Phys. Rev. C **34**, 746 (1986).
[47] Z. Yun *et al.*, Sci. China: Phys., Mech. Astron **57**, 1669 (2014).
[48] K. Kumar and M. Baranger, Nucl. Phys. A **110**, 529 (1968).
[49] K. Hara, A. Hayashi, and P. Ring, Nucl. Phys. A **385**, 14 (1982).
[50] Y. Shi, C. L. Zhang, J. Dobaczewski, and W. Nazarewicz, Phys. Rev. C **88**, 034311 (2013).
[51] M. Oi and P. M. Walker, Phys. Lett. B **576**, 75 (2003).
[52] H. Schnare, R. Schwengner, S. Frauendorf, F. Dönau, L. Käubler, H. Prade, A. Jungclaus, K. P. Lieb, C. Lingk, S. Skoda, J. Eberth, G. de Angelis, A. Gadea, E. Farnea, D. R. Napoli, C. A. Ur, and G. Lo Bianco, Phys. Rev. Lett. **82**, 4408 (1999).
[53] W. Pauli, in *Handbuck der Physik* (Springer-Verlag, Berlin, 1933), Vol. XXIV, p.120.
[54] D. R. Inglis, Phys. Rev. **96**, 1059 (1954).
[55] S. T. Balyaev, Mat.-Fys. Medd., K. Dan. Vidensk. Selsk. **31**, 11 (1959).
[56] A. Bohr and B. R. Mottelson, *Nuclear Structure* (Benjamin, New York, 1975), Vol. II.
[57] See, for example, K. Huang, *Statistical Mechanics*, 2nd ed. (Wiley & Sons., New York, 1987), Chap. 17.
[58] R. Aroumougame, N. Malhotra, S. S. Malik, and R. K. Gupta, Phys. Rev. C **35**, 994 (1987).